Chemical Engineering Journal 160 (2010) 370–377

Contents lists available at ScienceDirect

Chemical Engineering Journal

journal homepage: www.elsevier.com/locate/cej

Synthesis and characterization of carbon-modified titania photocatalysts with a hierarchical meso-/macroporous structure

Gao-Song Shao[a], Lei Liu[a], Tian-Yi Ma[a], Feng-Yun Wang[a], Tie-Zhen Ren[b], Zhong-Yong Yuan[a,*]

[a] Institute of New Catalytic Materials Science, Key Laboratory of Advanced Micro/Nanomaterials and Batteries/Cells (Ministry of Education), College of Chemistry, Nankai University, 94, Weijin Road, Tianjin 300071, PR China
[b] School of Chemical Engineering & Technology, Hebei University of Technology, Tianjin 300130, PR China

ARTICLE INFO

Article history:
Received 21 September 2009
Received in revised form 3 March 2010
Accepted 4 March 2010

Keywords:
Meso-/macroporous
Carbon-modified
Titania
Solar photocatalysis

ABSTRACT

Carbon-modified TiO_2 photocatalysts with a hierarchical meso-/macroporous structure were prepared through direct hydrolyzation of n-tetrabutyl titanate in the dodecylamine solution and subsequent calcination under nitrogen atmosphere. The resulting photocatalysts were characterized by X-ray diffraction, scanning and transmission electron microscopy, nitrogen sorption analysis, X-ray photoelectron spectroscopy, and UV–vis spectroscopy. A well-defined hierarchical macrochannel-like structure of mesoporous nanoparticle assembly with a predominant anatase phase was observed in the synthesized carbon-modified titania materials, exhibiting obviously high absorption in the wavelength range of 400–800 nm. It is revealed that carbon could not only substitute partly Ti in the form of Ti–O–C bond but also substitute O in the form of O–Ti–C, besides amorphous interstitial carbon atoms were synchronously introduced, benefitting the improvement of solar light photocatalytic activity. The synthesized hierarchical carbon-modified titanias materials exhibited excellent photocatalytic performance in the photodegradation of Rhodamine B dye, suggesting their promising potential as effective solar photocatalysts for organic waste degradation.

1. Introduction

Solar energy utilization and conversion attract much current interest. Many efforts have been devoted on the photocatalytic degradation of various organic and inorganic pollutants using solar or artificial light irradiation [1–5]. Semiconductor TiO_2 was considered as an excellent photocatalyst for the chemical utilization of solar energy [6–11], and doping with nonmetal elements, such as nitrogen, sulfur and carbon, was demonstrated to be an efficient way to promote titania-based photocatalyst sensitive to sunlight [12–16]. Carbon-doped titanias were even found to have higher photocatalytic activity than other doped ones under solar irradiation [15–19], stimulating many investigations on the synthesis and photocatalytic applications of carbon-doped titania photocatalysts, though the mechanism of C-doping in titania for photoactivity improvement is still not totally clear, and different understanding concerning the state and type of modified carbon to account for the photocatalytic activity of the C–TiO_2, such as substitutional carbon [14,17,18,20–22] (including Ti or O substitutional), interstitial carbon [15,17] or carbon–titania composites [23–26], can be seen in the literature.

The improvement of the photocatalytic activities could be also achieved by the structure modification of titania-based photocatalysts to have high specific surface area and large porosity [27,28]. Mesoporous carbon-doped TiO_2 [17] and C–TiO_2 nanocomposites [24] have been reported, exhibiting significantly high photocatalytic activity. However, high-surface-area nanocrystalline carbon-modified TiO_2 with a hierarchical porous structure was not reported yet to date, though the incorporation of light-harvesting macroporous channels into a mesoporous titania framework has recently been demonstrated to further increase its photocatalytic activity [29–32]. Interesting optical properties and photocatalytic activities in the visible light region have been observed in the hierarchical meso-/macroporous N- and P-doped titania materials [29,32]. In this contribution, we report the synthesis of carbon-modified meso-/macroporous titanias by a template-free spontaneous formation process. Their textural and structural properties were characterized, and their photocatalytic activities were evaluated under solar light-analog irradiation.

2. Experimental

2.1. Sample preparation

All chemicals were used as received, without further purification. 10 mL of tetrabutyl titanate (Kermel, A.R.) was mixed with

* Corresponding author. Tel.: +86 22 23509610; fax: +86 22 23509610.
E-mail address: zyyuan@nankai.edu.cn (Z.-Y. Yuan).

1385-8947/$ – see front matter © 2010 Elsevier B.V. All rights reserved.
doi:10.1016/j.cej.2010.03.011

0.041, 0.082 or 0.164 g of dodecylamine (*i.e.* 2×10^{-4}, 4×10^{-4} or 8×10^{-4} mol, in which the molar ratio of C atoms in dodecylamine and Ti atoms in tetrabutyl titanate (C/Ti) is 0.08, 0.16 or 0.32, respectively) at 40 °C, which was then dropwise added into a solution of 35 mL ethanol and 5 mL distilled water under slow stirring. After further stirring for three or more hours, the mixture was transferred into a Teflon-lined autoclave and heated statically in an oven at 80 °C for 2 days. The product was filtered, washed, and dried, which was then heated in a tubular furnace under N_2 atmosphere at 2 K/min from room temperature to 500 °C and maintained at 500 °C for 6 h, followed by air-cooling to room temperature. The collected product was labeled as C*x*Ti100 (*x* represents 100 times of C/Ti molar ratio in the synthesis mixture, *i.e.* 8, 16 or 32). For comparison, pure titania sample was prepared by the same method without adding dodecylamine, and labeled as C0Ti100.

2.2. Sample characterization

X-ray diffraction (XRD) patterns were collected on a Rigaku D/max-2500 diffractometer with Cu K_α radiation, operated at 40 kV and 100 mA.

N_2 adsorption–desorption isotherms were recorded on a Quantachrome NOVA 2000e sorption analyzer at liquid nitrogen temperature (77 K). The samples were degassed at 200 °C overnight prior to the measurement. The surface area was obtained by the Brunauer–Emmett–Teller (BET) method, and pore size distribution was calculated from the adsorption branch of the isotherms by the Barret–Joyner–Halenda (BJH) model.

Scanning electron microscopy (SEM) was taken on a Shimadzu SS-550 microscope at 15 keV. Transmission electron microscopy (TEM) was carried out on a Philips Tecnai G20 microscope, working at 200 kV. A trace amount of sample was dispersed in ethanol solution by sonication for 10 min, and then deposited on a carbon-coated copper grid, which was used as a TEM specimen.

Diffuse reflectance UV–vis absorption spectroscopy was employed on a JASCO V-570 UV–vis–NIR spectrophotometer over the wavelength range of 200–1000 nm, using $BaSO_4$ as a reference.

X-ray photoelectron spectroscopy (XPS) measurements were performed on a Kratos Axis Ultra DLD (delay line detector) spectrometer equipped with a monochromatic Al K_α X-ray source (1486.6 eV). All XPS spectra were recorded using an aperture slot of 300 μm × 700 μm, survey spectra were recorded with a pass energy of 160 eV, and high-resolution spectra with a pass energy of 40 eV.

2.3. Measurement of photocatalytic activity

The photocatalytic activity of the prepared samples was evaluated by the degradation of Rhodamine B (RhB) dye. A 200-W tungsten lamp was placed above a cylindrical vessel that surrounded by a circulating water jacket to cool it. The wavelength range of the tungsten bulb is usually considered as 400–2500 nm, which could be used roughly as a substitution of the solar light (wavelength range of about 380–2500 nm) for the solar light photocatalytic degradation process. 20 mg of the catalyst powder was placed into a 100 mL of RhB aqueous solution (1×10^{-5} mol/L, pH 6), and the lamp was located at 10 cm higher than the solution. All runs were conducted at ambient pressure and temperature. The suspensions were magnetically stirred in the dark for 30 min to ensure the establishment of an adsorption/desorption equilibrium, and then exposed to the light irradiation at room temperature. At given time intervals, about 5 mL of liquor was sampled, centrifuged for 5 min to discard any sediment. The absorbance of reaction solutions was measured using a SP-722 spectrometer at λ_{max} = 554 nm for RhB dye.

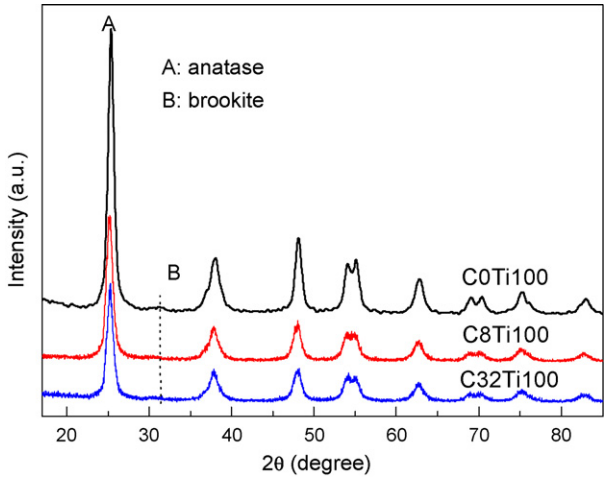

Fig. 1. The XRD pattern of the synthesized carbon-modified titania samples.

3. Results and discussion

3.1. Crystal structure, morphology and porosity

The autoclaving of the hydrolysis product of tetrabutyl titanate in the dodecylamine solution and the following calcination in the nitrogen atmosphere resulted in the formation of blackish-brown powders, and the XRD patterns of the synthesized C*x*Ti100 samples are shown in Fig. 1. The patterns of both pure and carbon-modified titania materials show mainly anatase phase, besides very trace quantities of brookite phase. No other phases such as carbon and TiC were observed. The presence of the trace quantities of brookite may benefit the photocatalytic performance of these materials, because the previously reported mixed crystalline titania structures showed outstanding optical properties [33–35]. A shift of the (1 0 1) peak of anatase from 25.24° to 25.16° (2θ) was observed in the carbon-modified titania, suggesting the surface strain and lattice distortion induced by the incorporation of carbon. A rough estimation of the

Table 1
Summary of the physicochemical properties of the synthesized samples.

Sample	S_{BET}[a] (m^2/g)	$D_{BJH\text{-}ads}$[b] (nm)	D_{ave}[c] (nm)	V_{pore}[d] (cm^3/g)	Crystallite size[e] (nm)	Lattice parameter (Å)		Degradation rate of RhB (k)
						a	c	
C0Ti100	103	5.8	5.9	0.15	10.7	3.7788	9.6244	4.2×10^{-3}
C8Ti100	81	3.0	3.4	0.068	9.2	3.7862	9.6702	8.0×10^{-3}
C16Ti100	69	2.4	3.3	0.055	–	–	–	9.9×10^{-3}
C32Ti100	59	2.2	3.2	0.048	9.1	3.7936	9.8324	5.4×10^{-3}

[a] BET surface area calculated from the linear part of the BET plot.
[b] Estimated using the adsorption branch of the isotherm by the BJH method.
[c] Average pore size calculated by the formula $D = 4V/A$, where A is surface area, V is the pore volume.
[d] Single point total pore volume of pores at $P/P_0 = 0.97$.
[e] Calculated by the Scherrer formula.

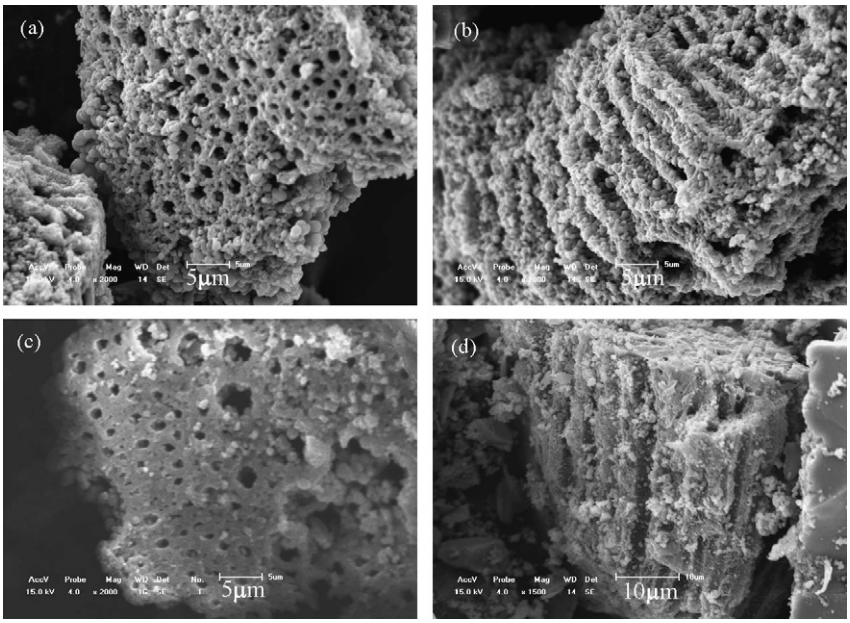

Fig. 2. SEM images of the (a and b) undoped titania C0Ti100 and (c and d) carbon-modified titania C16Ti100.

crystalline particle size using the Scherrer formula [36] from the (1 0 1) peaks of anatase is listed in Table 1. It is seen that the average crystallite sizes of the carbon-modified titanias are smaller than the pure titania. This indicates that the carbon modification could inhibit the growth of titania nanoparticles, in agreement with the case of some reported works [17,19], and the effect of carbon-doping is more pronounced than that of other anion doping, such as N-doping [19]. Based on Bragg' law ($2d\sin\theta = \lambda$) and a formula for a tetragonal system:

$$\frac{1}{d^2} = \frac{h^2 + k^2}{a^2} + \frac{l^2}{c^2}$$

the lattice parameters of TiO_2 samples were obtained and are listed in Table 1. The lattice parameter of carbon-modified titanias in the *c*-axis is larger than that of pure TiO_2 (C0Ti100) sample, indicating a lattice expansion along the *c*-axis due to the incorporation of carbon atoms. Under the carbonization process to replace oxygen atoms with carbon atoms, the oxygen vacancies and the interstitial carbon atoms would be formed, resulting in lattice mismatch and large internal stress, which might be the reason for the lattice parameter change in the synthesized carbon-modified titanias.

Fig. 2 shows the representative SEM images of the samples synthesized with or without carbon modification, revealing a uniform macroporous structure in all the samples. The macropores of pure titania sample C0Ti100 are channel-like with the size of 1–2 μm and the length of 15–20 μm, and the macrochannels are mainly of one-dimensional orientation, parallel to each other, perforative through the whole monolithic particles. And careful examination of these SEM micrographs reveals that the walls of the macropores are composed of small interconnected granular particles, leaving small holes of 100–500 nm in the macropore walls. The carbon-modified titania C*x*Ti100 has the similar macroporous structure with the unmodified one, but less uniform, with the macropore sizes in the range of 1–1.5 μm and the length of up to around 30 μm.

The N_2 adsorption–desorption isotherms and the corresponding pore size distributions of the synthesized C*x*Ti100 catalysts are shown in Fig. 3, and their textural properties are listed in Table 1. The isotherms recorded for these materials correspond to Type IV adsorption isotherms according to the IUPAC, which are characteristic of mesoporous materials [37,38]. The well-defined hysteresis loops with a steep desorption branch and less steep adsorption branch belong to the H2-type, indicating that the effective radii of the mesoporous bodies are heterogeneously distributed and the effective radii of the narrow entrance are all of equal size [39]. The pore size distribution curve of the C0Ti100 sample, determined by the BJH method from the adsorption branch of the isotherms, displays one single distribution peak in the range of 2–11 nm, centered at 5.9 nm. However, the pore size distributions narrowed after carbon modification, and the distribution peak vertexes shifted to 3.4, 3.3 and 3.2 nm for the samples C8Ti100, C16T100 and C32Ti100, respectively, indicating the effect of carbon modification on the mesoporosity of the resultant hierarchical materials. Furthermore, with the increase of C/Ti ratio, the hysteresis loop tends to gradually reduce, even disappear, suggesting the decrease of capillary condensation and the uniformization of channel-like mesopores due to the effect of carbon-doping. Much uniform mesoporous structures can be expected in the carbon-modified titania samples, which might be the assistance effects of surfactant dodecylamine during the formation of mesostructure [40–42]. With the increase of the carbon content, the pore sizes and the BET surface areas decreased, accompanied with the decrease of the pore volume (Table 1), which may be the result of the existence of the carbon species on the surfaces of the synthesized C*x*Ti100 samples.

Such a uniform mesoporosity in these pure and carbon-modified titania materials determined by the N_2-sorption analysis was further confirmed by the TEM observation (Fig. 4). The fine particulate morphology between the macrochannels of pure and carbon-modified titanias is clearly displayed on their TEM images in Fig. 4, demonstrating that all the C*x*Ti100 samples had a disordered wormhole-like mesoporous structure that was formed by the aggregation of nanoparticles with the size of about 10 nm. The accessible pores are connected randomly, lacking discernible long-range order in the pore arrangement among the small particles, in well agreement with the N_2 adsorption–desorption isotherms, as well as low angle X-ray diffraction patterns that did not show any significant diffraction peaks at 2θ of 1–3° (not shown). The observed mesoporosity is probably partly due to the intraparticle porosity and partly due to the interparticle porosity [43]. Thus, the synthesized carbon-modified titania catalysts have a porous hierarchy of mesoporous–macroporous structure.

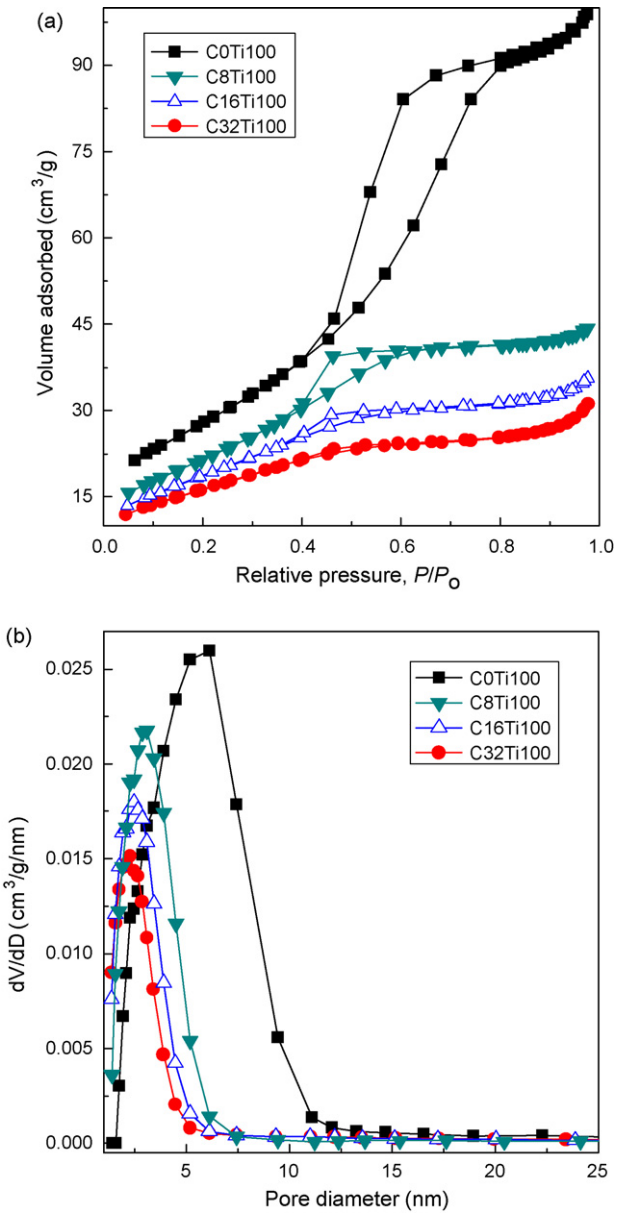

Fig. 3. (a) N_2 adsorption–desorption isotherms and (b) the corresponding BJH pore size distribution curves of the prepared samples.

Since both pure titania and carbon-modified titanias have a hierarchical meso-/macroporous structure, and their synthesis process was carried out in the absence of any templates, the formation mechanism of such meso-/macrostructures is followed by a spontaneous self-assembly process, as described previously [32,44–46]. The hydrolysis of Ti-alkoxide precursors in the dodecylamine solution would result in the rapid formation of nanometer-sized titanium oxide oligomer particles attached with dodecylamine molecules. Meanwhile, many alcohol molecules were generated quickly as by-product, which might produce microphase-separated domains of dodecylamine-containing titania-based nanoparticles and water/alcohol channels that are the initiators and the driving force for the formation of the macrochannels. Those titanium oxide oligomers go on hydrolyzation and polycondensation into the mesostructured dodecylamine-modified titania nanoparticles. Dodecylamine surfactant-assisted synthesis of mesoporous oxides has been reported elsewhere [40–42]. Thus, a hierarchical structure of uniform macrochannels with mesopores walls of nanoparticle assembly would form during the synergistic packing of the nanoparticles and rapid release of alkanol molecules. The subsequent calcination at nitrogen atmosphere can result in carbon incorporation in the titania framework of the hierarchical meso-/macroporous structures, as well as the possible coke-like carbonaceous species at the surface of titania nanoparticles. The carbonaceous species also acts as a glue linking with the TiO_2 nanocrystals by covalent bonds or the coordination between Ti and HO–C groups [24], benefitting the nanoparticle assembly and uniformization of mesopores.

3.2. Chemical structure and compositions

High-resolution XPS measurement was carried out to investigate the carbon, titanium and oxygen state and relative carbon content of the synthesized carbon-modified titania materials. Fig. 5 shows the Ti 2p, O 1s and C 1s XPS spectra of the C*x*Ti100 samples, and Table 2 lists the measured binding energies and the contents of carbon atoms. In the Ti 2p spectra (Fig. 5a), the Ti $2p_{3/2}$ peak situated at 458.6 eV with a shoulder around 457 eV while the Ti $2p_{1/2}$ peak presented at 464.4 eV with a shoulder around 463 eV. The main Ti $2p_{3/2}$ peaks at 458.6 eV and Ti $2p_{1/2}$ peaks at 464.4 eV are characteristic of Ti^{4+} [47]. The shoulders of Ti $2p_{3/2}$ and Ti $2p_{1/2}$ at around 457 and 463 eV, respectively, suggest that Ti^{3+} species were formed in the carbon-modified titania, which could be attributed to a partial reduction of Ti^{4+} to Ti^{3+} by carbon species under N_2 atmosphere. The emergence of Ti^{3+} species would result in the formation of surface oxygen vacancies [15,48].

The chemical environment of Ti is significantly influenced by its coordination environment. Compared with the binding energy of pure TiO_2 (459 eV for $Ti2p_{3/2}$ and 464.8 eV for $Tip_{1/2}$), the binding energy of Ti^{4+} 2p in the carbon-modified titania samples is lower than that in pure TiO_2. This is the result from different electronic interactions of Ti with anions, which causes partial electron transformation from C to Ti and an increase of the electron density on Ti because of the lower electronegativity of carbon compared with oxygen (O > C). Therefore, the lower binding energy is also ascribed to the forming of new bond O–Ti–C, where some oxygen was substituted partly by the carbon [20,21].

The XPS spectra of O 1s (Fig. 5b) could be mainly fitted into three peaks. The binding energy at round 530.0 eV is ascribed to the oxygen in Ti–O bonds [16,20,49], while the O 1s signal at round 532.0 eV could be attributed as the hydroxyl groups or the C–O bonds, deducing the existence of Ti–O–C bonds. An additional peak at low binding energy of 528.0 eV, unambiguously ascribed to the O atoms bonded with Ti^{3+} [50], is seen in the spectrum of sample C8Ti100, but unconspicuous in the samples C16Ti100 and C32Ti100, suggesting that the Ti^{3+} contents in C16Ti100 and C32Ti100 are smaller than that in C8Ti100.

The carbon states in the photocatalysts could be investigated from C 1s core levels, as shown in Fig. 5c. Four peaks are observed in the C 1s spectra of the hierarchical C*x*Ti100 samples. The peak at the binding energy of 284.6 eV is the strongest among those fitted peaks and is thought to signal the presence of elemental carbon including the coke-like carbonaceous species at the surface of titania nanoparticles, amorphous interstitial carbon atoms, as well as adventitious carbon [15,17]. The peaks around 286.6 and 288.3 eV indicate the presence of C–N and C–O bonds [51]. The nitrogen atoms in the C–N bonds might also be from the precursor organic compound DDA, though the N contents in the resultant C*x*Ti100 photocatalysts are very low (0.15%, 0.35% and 0.52% on the surface of C8Ti100, C16Ti100 and C32Ti100, respectively). This suggests that carbon may substitute for some of the lattice titanium atoms and form a Ti–O–C structure [15,17], as well as the nitrogen doping in the synthesized C-modified titanias. Meanwhile, the peak around 282.8 eV could be assigned to O–Ti–C bond

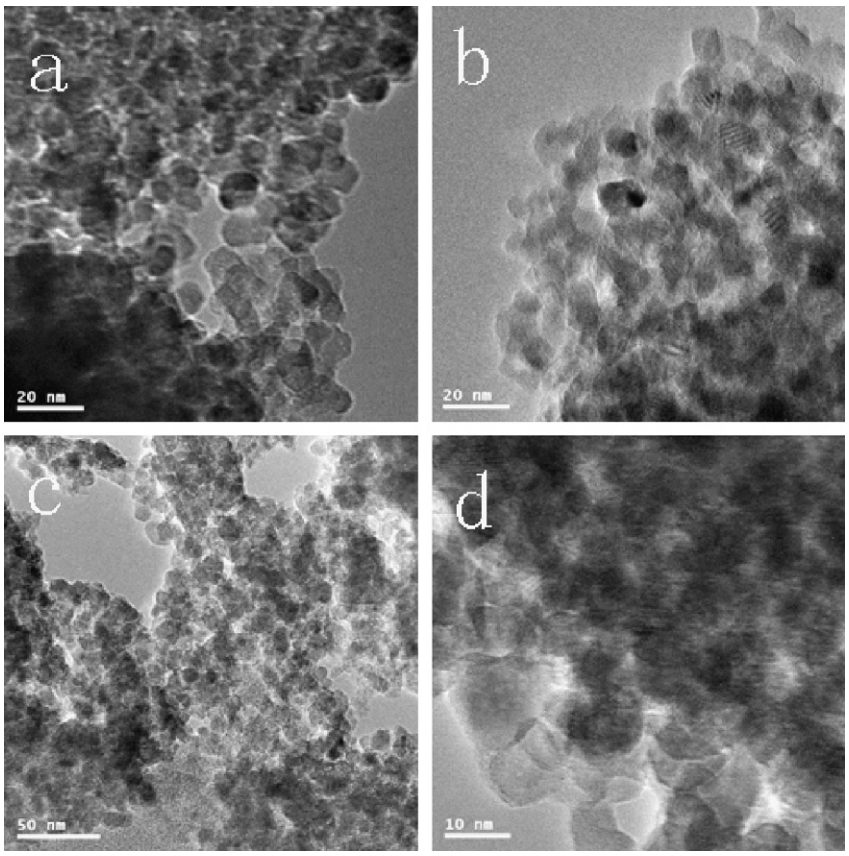

Fig. 4. TEM images of titania materials (a and b) C0Ti100 and (c and d) C16Ti100.

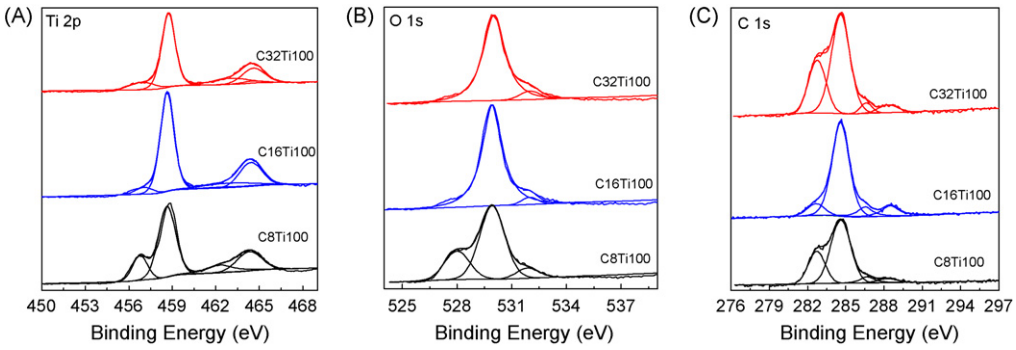

Fig. 5. XPS analysis of catalysts: (a) the Ti 2p spectrum, (b) the O 1s spectrum, and (c) the C 1s spectrum.

Table 2
Summary of the binding energy and the mass content of carbon atoms by XPS analysis.

Sample	Ti 2p binding energy (eV)				O 1s binding energy (eV)			C 1s binding energy (eV)				O/Ti	C/Ti
C32Ti100	456.9	458.7	463.0	464.6	530.0	532.0	–	282.8	284.6	286.6	288.4	2.99	4.83
C16Ti100	457.0	458.6	462.9	464.4	529.9	531.9	–	282.7	284.6	286.5	288.5	2.43	2.49
C8Ti100	456.8	458.6	462.3	464.3	528.0	529.9	531.9	282.7	284.6	286.7	288.2	2.43	2.24

[20,21] in carbon-modified titania by substituting some of the lattice oxygen atom with carbon. Thus, four kinds of carbon species exist: carbon, O–Ti–C, Ti–O–C and C–N, whose contents gradually reduce in order. The total surface carbon mass concentrations in the samples C8Ti100, C16Ti100 and C32Ti100 were estimated from XPS spectra to be 23.6%, 25.5% and 37.5%, respectively. The total contents of carbon atoms (Table 2) are much larger than the carbon source of dodecylamine added in the synthesis system, which may be the results that both dodecylamine and tetrabutyl titanate itself, as well as the organic solvent in the synthesis system, can be regarded as carbon precursors, all contributing the carbon content in the resultant samples, though the adsorbed carbon pollution on the surface of samples cannot be excluded. Also the XPS can only detect a very thin surface layer of the particles, and the carbon species located on the surface of the samples are much larger than that incorporated in the lattice of titania, giving a presentational XPS data of large carbon content in the resultant samples.

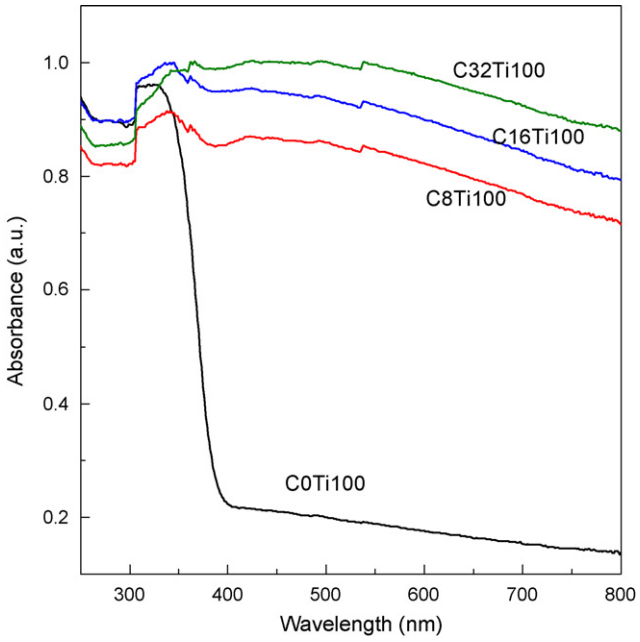

Fig. 6. UV–vis absorption spectra of synthesized samples.

The presence of some carbon species in titania is proposed to be responsible for the visible light photoactivity. However, the chemical nature of the "carbon dopant" is still a matter of discussion. Sakthivel and Kisch [18] believed that carbon modification was cation doping, which was beneficial to improve photocatalytic activity. Ren et al. [17] reported that carbon substituted for some of the lattice titanium atoms to form new Ti–O–C bond. However, some other researchers [20–22] thought carbon substituted for some of the lattice oxygen atoms. While Wu et al. [14] observed O–Ti–C and Ti–O–C bonds in their carbon-doped TiO_2 nanostructures, and believed carbon-doping was both cation and anion doping. In the present meso-/macroporous C*x*Ti100 samples, as revealed from the XPS spectra, carbon could substitute partly for Ti in form of Ti–O–C bond and could substitute partly for O in the form of O–Ti–C, which is consistent with the case of Wu et al. [14]. Given the relatively small size of the C atom, Valentin et al. [52] also predicted that it is an unexpected stabilization and feasibility induced by multidoping effects (Ti and O substitutional) using density functional theory calculations. Meanwhile, amorphous interstitial carbon atoms (or coke-like carbonaceous species [26,53]) were also embedded in C*x*Ti100 samples, and/or on the surface of the TiO_2 crystallites just like "coats", which could contribute to absorption of light in the visible region.

3.3. Optical property and photocatalytic activity

UV–vis diffuse reflectance spectra of the pure and carbon-modified titania are shown in Fig. 6. The onset of the absorption spectrum of the synthesized pure meso-/macroporous titania (C0Ti100) appeared at about 400 nm. After carbon modification with different carbon contents, the color of samples changed from brown into blackish-brown, and the resultant C-modified titanias appear to be quite different from unmodified titania with their distinctly great absorption in the visible light region. The absorption edges for C-modified titania samples shift greatly toward a larger wavelength (>800 nm). Such an absorption feature suggests that the carbon-modified titanias can be activated by visible light. One reason for the broad absorbance may be the existence of residual carbon, though the effect of real carbon modification to extend the adsorption to visible light range cannot be ignored. Xiao et al. [16],

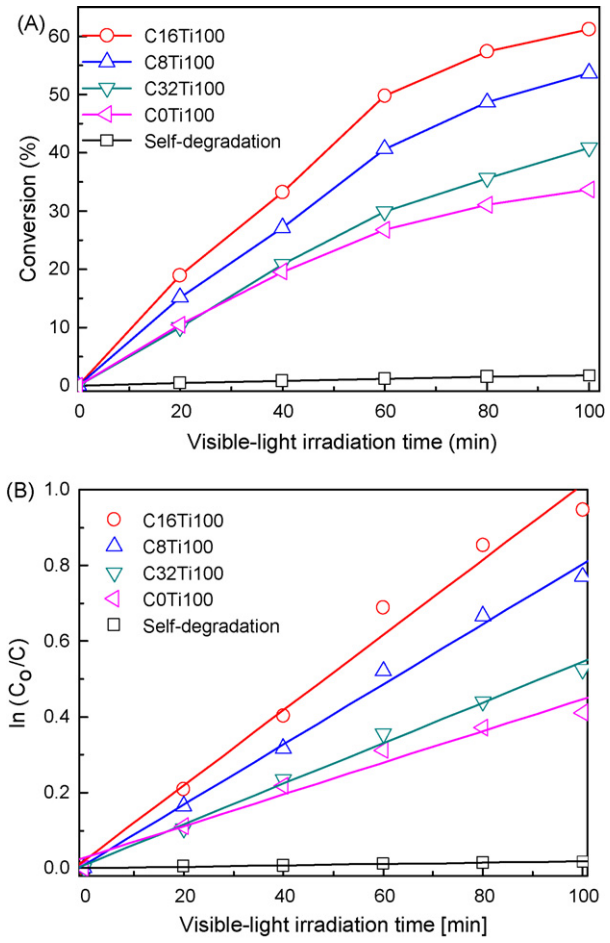

Fig. 7. (a) The photoactivity of the catalysts C*x*Ti100 for RhB photodecomposition under tungsten bulb light irradiation; (b) a plot of ln (C_0/C) versus the irradiation time, showing the fitting results using the pseudo-first-order reaction.

Li et al. [15] and Yang et al. [51] prepared carbon-doped titania and found these materials exhibited the new absorption at visible light range, which can be ascribed to the presence of oxygen vacancy state because of the formation of Ti^{3+} species, and the doping of carbon state between the valence and the conduction bands.

The strong absorption in the wavelength of 420–800 nm corresponding to the band gap of 2.95–1.55 eV should be related to the formation of O–Ti–C [20–22] or Ti–O–C bands [17,18,51] or/and presence of oxygen vacancy states due to the formation of Ti^{3+} species [15,16,51] which are located above the O 2p-based valence band, besides the surface carbonaceous species. Yang and coworkers [22] observed about 36 nm of red-shift in their C–TiO_2 samples, and the change of the spectra could be attributed to ca. 0.7 wt.% carbon substitutions at oxygen sites. Wu et al. [14] found their synthesized carbon-modified titania nanomaterials with narrowing band gap showed a huge absorbance in the whole visible light region. The band gap narrowing could be attributed to the substitutional carbon for oxygen, which resulted in the upward shift of the valence band top [14,52]. The long-tail absorption in the visible region can be attributed to the existence of carbonate species [14]. Also it has another possible case that the mixed phase (anatase and brookite) surface structures effectively reduced the band gap by introducing some interface states in synthesized samples [54].

The photocatalytic activities of the obtained meso-/macroporous carbon-modified titanias were investigated by the degradation of RhB under tungsten bulb light irradiation, an analog of solar light irradiation, and the results are shown in Fig. 7. In order to make sure the important roles of catalyst, a blank

experiment (self-photosensitized process, in the absence of any catalysts) was performed under identical conditions. As shown in Fig. 7a, self-degradation process is inactive, as evidenced by only 1.7% of RhB degraded after 100 min of tungsten bulb light irradiation. However, the degradation rate increased greatly after adding catalysts. The RhB conversions of 61.2%, 53.7%, 40.9% and 33.7% are obtained for the samples C16Ti100, C8Ti100, C32Ti100 and C0Ti100, respectively. The carbon-modified titanias have higher photocatalytic abilities than the pure TiO_2. The activity of sample C16Ti100 is almost twice as high as that of pure titania C0Ti100. Strong light absorption has been observed in the carbon-modified titanias, and larger red-shift of valence band produced due to carbon-doping, compared with the case of other anion (such as N, S, etc.) doped titanias [19,55], which are all favorable to improve the catalytic activity. Wang and Lewis [55] made a systematic study about anion-doped TiO_2, and believed that carbon-doped TiO_2 was very promising due to a significant overlap between the O 2p state and the carbon states near the valence band edge. Nevertheless, the sample C32Ti100 has the highest carbon content in the prepared carbon-modified titanias, but showed the lowest photocatalytic activity, indicating that excessive carbon modification is disadvantageous to the photodegradation of organic substrates. The existence of carbonaceous species at the surface for hierarchical C*e*Ti100 photocatalyst lowered its photocatalytic activity due to absorption of visible light by the carbonaceous species and consequently reduced the fraction of visible photons available for the covered C*e*Ti100 photocatalyst to generate electron–hole pairs [53]. It is important to note that it is photogenerated holes that are mainly responsible for the degradation of organics or the photocatalytic activity [53].

The photocatalytic degradation reaction can be assumed to follow a pseudo-first-order expression: $\ln(C_0/C) = kt$, where C_0/C is the normalized organic compounds concentration and k is the apparent reaction rate constant (min^{-1}). The photocatalytic activity has been defined as the overall degradation rate constant of the catalysts. By plotting $\ln(C_0/C)$ as a function of irradiation time through regression (Fig. 7b), the k constant from the slopes of the simulated straight lines is obtained, and listed in Table 1. The value of k increases from 4.2×10^{-3} to 8.0×10^{-3} and to 9.9×10^{-3} min^{-1} when the C/Ti ratios in the catalyst synthesis system increased from 0 to 0.08 and to 0.16. However, further increasing the C/Ti ratio in the catalyst synthesis system to 0.32, the k value decreased to 5.4×10^{-3} min^{-1}. It is noted that the k value of the catalyst C16Ti100 is nearly twice of that of previously reported nitrogen doped titania (5.3×10^{-3} min^{-1}) [32].

Several reasons may account for the high photoactivity of the hierarchical carbon-modified titanias. First, the synthesized carbon-modified titania materials possess hierarchical meso-/macroporous structures that could achieve highly organized functions. Macropores in mesoporous materials could give enhanced properties due to increasing mass transport through the material and maintenance of a specific surface area on the level of fine system. Also the macroporous channels could serve as light-transfer paths for the distribution of photon energy onto the large surface of inner photoactive mesoporous frameworks. Our previous work [32] has clearly certificated the effects of macrochannels by a significant drop in photocatalytic activity of the catalyst with only mesoporous structure but without macrochannels. Second, after carbon modification, the carbon was the gap-filling atoms and some new bonds formed, such as Ti–O–C or O–Ti–C, and the modification results will inevitably form Ti^{3+}, giving rise to a small number of oxygen vacancies, which is beneficial to photocatalytic activity. Third, the framework of carbon modification titania has some amorphous carbon that could increase the adsorption capacity and light absorption as the sensitizer of the solar light, and also serve as the scavenger of electrons to inhibit the recombination of the photogenerated carriers [23,56]. The photocatalytic performance may also be ascribed to the synergistic effect that the amorphous carbon adsorbs more organic substrates followed by a transfer to the photocatalytic active titania surface for the decomposition of organic molecules under solar light [23,57]. Fourth, the existence of small quantity of brookite phase in the synthesized C*x*Ti100 samples, forming a bicrystalline (anatase and brookite) structure, which also benefit their photocatalytic activity [33–35].

4. Conclusions

Hierarchical meso-/macroporous carbon-modified titania materials have been synthesized successfully without any templates, presenting the structural feature of bicrystalline (anatase and brookite) phase, hierarchical porous structure, high-surface-area and uniform mesopore size distribution. The incorporation of carbon into the titania lattice was confirmed by forming Ti–O–C and O–Ti–C bonds, besides amorphous interstitial carbon atoms and surface carbonaceous materials. The strong absorbance in the visible to near infrared region was observed in the synthesized meso-/macroporous C*x*Ti100 samples. Compared with undoped titania, the synthesized carbon-modified titanias exhibited significantly higher photocatalytic activity in the photodegradation of RhB under solar light-analog irradiation, suggesting their potential in the solar light utilization for photodegradation of toxic organic waste.

Acknowledgements

This work was supported by the National Natural Science Foundation of China (20803017, 20973096), the National Basic Research Program of China (2009CB623502), the Specialized Research Fund for the Doctoral Program of Higher Education (20070055014), the Natural Science Foundation of Tianjin (08JCZDJC21500), the Program for New Century Excellent Talents in University (NCET-06-0215), and Nankai University.

References

[1] A.I. Gomes, J.C. Santos, V.J.P. Vilar, R.A.R. Boaventura, Inactivation of bacteria *E. coli* and photodegradation of humic acids using natural sunlight, Appl. Catal. B: Environ. 88 (2009) 283–291.
[2] J.J. Xu, Y.H. Ao, D.G. Fu, C.W. Yuan, Study on photocatalytic performance and degradation kinetics of X-3B with lanthanide-modified titanium dioxide under solar and UV illumination, J. Hazard. Mater. 164 (2009) 762–768.
[3] S. Kaneco, N. Li, K. Itoh, H. Katsumata, T. Suzuki, K. Ohta, Titanium dioxide mediated solar photocatalytic degradation of thiram in aqueous solution: kinetics and mineralization, Chem. Eng. J. 148 (2009) 50–56.
[4] S.K. Pardeshi, A.B. Patil, Solar photocatalytic degradation of resorcinol a model endocrine disrupter in water using zinc oxide, J. Hazard. Mater. 163 (2009) 403–409.
[5] D. Bircan, S. Ozlem, Photodegradation of 2,4-dichlorophenoxy acetic acid on TiO_2, ZnO and Fe_2O_3 by sunlight, Asian J. Chem. 21 (2009) 2270–2282.
[6] M. Stylidi, D.I. Kondarides, X.E. Verykios, Pathways of solar light-induced photocatalytic degradation of azo dyes in aqueous TiO_2 suspensions, Appl. Catal. B: Environ. 40 (2003) 271–286.
[7] J.M. Herrmann, C. Guillard, J. Disdier, C. Lehaut, S. Malato, J. Blanco, New industrial titania photocatalysts for the solar detoxification of water containing various pollutants, Appl. Catal. B: Environ. 35 (2002) 281–294.
[8] A.A. Yawalkar, D.S. Bhatkhande, V.G. Pangarkar, A.A.C.M. Beenackers, Solar-assisted photochemical and photocatalytic degradation of phenol, J. Chem. Technol. Biotechnol. 76 (2001) 363–370.
[9] W.S. Kuo, P.H. Ho, Solar photocatalytic decolorization of methylene blue in water, Chemosphere 45 (2001) 77–83.
[10] D. Robert, S. Malato, Solar photocatalysis: a clean process for water detoxification, Sci. Total Environ. 291 (2002) 85–97.
[11] D.S. Bhatkhande, V.G. Pangarkar, A.A.C.M. Beenackers, Photocatalytic degradation of nitrobenzene using titanium dioxide and concentrated solar radiation: chemical effects and scaleup, Water Res. 37 (2003) 1223–1230.
[12] Y. Liu, X. Chen, J. Li, C. Burda, Photocatalytic degradation of azo dyes by nitrogen-doped TiO_2 nanocatalysts, Chemosphere 61 (2005) 11–18.
[13] T. Ohnoa, M. Akiyoshi, T. Umebayashi, K. Asai, T. Mitsui, M. Matsumura, Preparation of S-doped TiO_2 photocatalysts and their photocatalytic activities under visible light, Appl. Catal. A: Gen. 265 (2004) 115–121.

[14] Z.B. Wu, F. Dong, W.R. Zhao, H.Q. Wang, Y. Liu, B.H. Guan, The fabrication and characterization of novel carbon doped TiO_2 nanotubes, nanowires and nanorods with high visible light photocatalytic activity, Nanotechnology 20 (2009) 235701–235709.
[15] Y.Z. Li, D.S. Hwang, N.H. Lee, S.J. Kim, Synthesis and characterization of carbon-doped titania as an artificial solar light sensitive photocatalyst, Chem. Phys. Lett. 404 (2005) 25–29.
[16] Q. Xiao, J. Zhang, C. Xiao, Z.C. Si, X.K. Tan, Solar photocatalytic degradation of methylene blue in carbon-doped TiO_2 nanoparticles suspension, Solar Energy 82 (2008) 706–713.
[17] W.J. Ren, Z.H. Ai, F.L. Jia, L.Z. Zhang, X.X. Fan, Z.G. Zou, Low temperature preparation and visible light photocatalytic activity of mesoporous carbon-doped crystalline TiO_2, Appl. Catal. B: Environ. 69 (2007) 138–144.
[18] S. Sakthivel, H. Kisch, Daylight photocatalysis by carbon-modified titanium dioxide, Angew. Chem. Int. Ed. 42 (2003) 4908–4911.
[19] D.M. Chen, Z.Y. Jiang, J.Q. Geng, Q. Wang, D. Yang, Carbon and nitrogen co-doped TiO_2 with enhanced visible-light photocatalytic activity, Ind. Eng. Chem. Res. 46 (2007) 2741–2746.
[20] H. Irie, Y. Watanabe, K. Hashimoto, Carbon-doped anatase TiO_2 powders as a visible-light sensitive photocatalyst, Chem. Lett. 32 (8) (2003) 772–773.
[21] S.U.M. Khan, M. Al-Shahry, W.B. Ingler, Efficient photochemical water splitting by a chemically modified n-TiO_2, Science 297 (2002) 2243–2245.
[22] M. Shen, Z. Wu, H. Huang, Y. Du, P. Yang, Carbon-doped anatase TiO_2 obtained from TiC for photocatalysis under visible light irradiation, Mater. Lett. 60 (2006) 693–697.
[23] M. Li, S.F. Zhou, Y.W. Zhang, G.Q. Chen, Z.L. Hong, One-step solvothermal preparation of TiO_2/C composites and their visible-light photocatalytic activities, Appl. Surf. Sci. 254 (2008) 3762–3766.
[24] R.L. Liu, Y.J. Ren, Y.F. Shi, F. Zhang, L.J. Zhang, B. Tu, D.Y. Zhao, Controlled synthesis of ordered mesoporous C–TiO_2 nanocomposites with crystalline titania frameworks from organic–inorganic-amphiphilic coassembly, Chem. Mater. 20 (2008) 1140–1146.
[25] M. Janus, B. Tryba, M. Inagaki, A.W. Morawski, New preparation of a carbon-TiO_2 photocatalyst by carbonization of n-hexane deposited on TiO_2, Appl. Catal. B: Environ. 52 (2004) 61–67.
[26] C. Lettmann, K. Hildenbrand, H. Kisch, W. Macyk, W.F. Maier, Visible light photodegradation of 4-chlorophenol with a coke-containing titanium dioxide photocatalyst, Appl. Catal. B: Environ. 32 (2001) 215–227.
[27] T.Y. Peng, D. Zhao, K. Dai, W. Shi, K. Hirao, Synthesis of titanium dioxide nanoparticles with mesoporous anatase wall and high photocatalytic activity, J. Phys. Chem. B 109 (2005) 4947–4952.
[28] L. Körösi, I. Dékány, Preparation and investigation of structural and photocatalytic properties of phosphate modified titanium dioxide, Colloids Surf. A: Physicochem. Eng. Aspects 280 (2006) 146–154.
[29] G.-S. Shao, T.-Y. Ma, X.-J. Zhang, T.-Z. Ren, Z.-Y. Yuan, Phosphorus and nitrogen co-doped titania photocatalysts with a hierarchical meso-/macroporous structure, J. Mater. Sci. (2009) 3628–3630, doi:10.1007/s10853-009-3628-z.
[30] X. Wang, J.C. Yu, C. Ho, Y. Hou, X. Fu, Photocatalytic activity of a hierarchically macro/mesoporous titania, Langmuir 21 (2005) 2552–2559.
[31] J.G. Yu, L.J. Zhang, B. Cheng, Y.R. Su, Hydrothermal preparation and photocatalytic activity of hierarchically sponge-like macro-/mesoporous titania, J. Phys. Chem. C 111 (2007) 10582–10589.
[32] G.S. Shao, X.J. Zhang, Z.Y. Yuan, Preparation and photocatalytic activity of hierarchically mesoporous-macroporous $TiO_{2-x}N_x$, Appl. Catal. B: Environ. 82 (2008) 208–218.
[33] X.J. Ye, D. Chen, K.Y. Li, V. Shah, Photocatalytic oxidation of aldehydes/PCE using porous anatase titania and visible-light-responsive brookite titania, Chem. Eng. Commun. 194 (2007) 368–381.
[34] S.S. Yan, L.D. Wu, F. Chen, J.L. Zhang, Low-temperature preparation and characterization of TiO_2 thin films with a bicrystalline framework, Acta Phys. Chim. Sin. 23 (2007) 414–418.
[35] L.J. Zhou, S.S. Yan, B.Z. Tian, F. Chen, J.L. Zhang, J.Z. Huang, Preparation and characterization of anatase-brookite TiO_2 film on the PET surface, Acta Phys. Chim. Sin. 22 (2006) 569–573.
[36] H.P. Klug, L.E. Alexander, X-ray Diffraction Procedure for Polycrystalline and Amorphous Materials, 2nd ed., Wiley, New York, 1974.
[37] K.S.W. Sing, D.H. Evett, R.A.W. Haul, L. Moscou, R.A. Pierotti, J. Rouquerol, T. Siemieniewska, Reporting physisorption data for gas/solid systems with special reference to the determination of surface area and porosity, Pure Appl. Chem. 57 (1985) 603–619.
[38] M. Kruk, M. Jaroniec, Gas adsorption characterization of ordered organic–inorganic nanocomposite materials, Chem. Mater. 13 (2001) 3169–3183.
[39] T.Z. Ren, Z.Y. Yuan, B.L. Su, Surfactant-assisted preparation of hollow microspheres of mesoporous TiO_2, Chem. Phys. Lett. 374 (2003) 170–175.
[40] D.M. Antonelli, Synthesis of phosphorus-free mesoporous titania via templating with amine surfactants, Micropor. Mesopor. Mater. 30 (1999) 315–319.
[41] P.T. Tanev, T.J. Pinnavaia, Mesoporous silica molecular sieves prepared by ionic and neutral surfactant templating: a comparison of physical properties, Chem. Mater. 8 (1996) 2068–2079.
[42] Y.Q. Wang, X.H. Tang, L.X. Yin, W.P. Huang, Y.R. Hacohen, A. Gedanken, Sonochemical synthesis of mesoporous titanium oxide with wormhole-like framework structures, Adv. Mater. 12 (2000) 1183–1186.
[43] Z.Y. Yuan, T.Z. Ren, A. Azioune, J.J. Pireaux, B.L. Su, Self-assembly of hierarchically mesoporous-macroporous phosphated nanocrystalline aluminum (oxyhydr)oxide materials, Chem. Mater. 18 (2006) 1753–1767.
[44] A. Collins, D. Carriazo, S.A. Davis, S. Mann, Spontaneous template-free assembly of ordered macroporous titania, Chem. Commun. (2004) 568–569.
[45] T.Z. Ren, Z.Y. Yuan, B.L. Su, Thermally stable macroporous zirconium phosphates with supermicroporous walls: a self-formation phenomenon of hierarchy, Chem. Commun. (2004) 2730–2731.
[46] T.Z. Ren, Z.Y. Yuan, A. Azioune, J.J. Pireaux, B.L. Su, Tailoring the porous hierarchy of titanium phosphates, Langmuir 22 (2006) 3886–3894.
[47] L. Ramqvist, K. Hamrin, G. Johansson, A. Fahlmann, C. Nordling, Charge transfer in transition metal carbides and related compounds studied by ESCA, J. Phys. Chem. Solids 30 (1969) 1835–1847.
[48] X.Y. Du, Y. Wang, Y.Y. Mu, L.L. Gui, P. Wang, Y.Q. Tang, A new highly selective H_2 sensor based on TiO_2/PtO–Pt dual-layer films, Chem. Mater. 14 (2002) 3953–3957.
[49] K. Nagaveni, M.S. Hegde, N. Ravishankar, G.N. Subbanna, G. Madras, Synthesis and structure of nanocrystalline TiO_2 with lower band gap showing high photocatalytic activity, Langmuir 20 (2004) 2900–2907.
[50] P.M. Kumar, S. Badrinarayanan, M. Sastry, Nanocrystalline TiO_2 studied by optical, FTIR and X-ray photoelectron spectroscopy: correlation to presence of surface states, Thin Solid Films 358 (2000) 122–130.
[51] J. Yang, H.Z. Bai, X.C. Tan, J.S. Lian, IR and XPS investigation of visible-light photocatalysis—nitrogen–carbon-doped TiO_2 film, Appl. Surf. Sci. 253 (2006) 1988–1994.
[52] C.D. Valentin, G. Pacchioni, A. Selloni, Theory of carbon doping of titanium dioxide, Chem. Mater. 17 (2005) 6656–6665.
[53] C. Xu, R. Killmeyer, M.L. Gray, S.U.M. Khan, Photocatalytic effect of carbon-modified n-TiO_2 nanoparticles under visible light illumination, Appl. Catal. B: Environ. 64 (2006) 312–317.
[54] P.W. Chou, S. Treschev, P.H. Chung, C.L. Cheng, Y.H. Tseng, Y.J. Chen, M.S. Wong, Observation of carbon-containing nanostructured mixed titania phases for visible-light photocatalysts, Appl. Phys. Lett. 89 (2006) 131919(1)–131919(3).
[55] H. Wang, J.P. Lewis, Second-generation photocatalytic materials: anion-doped TiO_2, J. Phys.: Condens. Matter 18 (2006) 421–434.
[56] M. Janus, M. Inagaki, B. Tryba, M. Toyoda, A.W. Morawski, Carbon-modified TiO_2 photocatalyst by ethanol carbonization, Appl. Catal. B: Environ. 63 (2006) 272–276.
[57] T. Tsumura, N. Kojitani, I. Izumi, N. Iwashita, M. Toyoda, M. Inagaki, Carbon coating of anatase-type TiO_2 and photoactivity, J. Mater. Chem. 12 (2002) 1391–1396.